Tuning the supramolecular isomerism of MOF-74 by controlling the synthesis conditions

Andreea Gheorghe[†], *Inhar Imaz*[‡], *Jarl Ivar van der Vlugt*[§], *Daniel Maspoch*[‡,⊥], *and Stefania Tanase**[†]

[†]Heterogeneous Catalysis and Sustainable Chemistry, [§]Bioinspired, Homogeneous & Supramolecular Catalysis, van 't Hoff Institute for Molecular Sciences, University of Amsterdam, Science Park 904, 1098 XH Amsterdam, The Netherlands

[‡] Catalan Institute of Nanoscience and Nanotechnology (ICN2), CSIC and Barcelona Institute of Science and Technology, Campus UAB, Bellaterra 08193, Barcelona, Spain

[⊥]ICREA, Pg. Lluís Companys 23, 08010 Barcelona, Spain

ABSTRACT: Supramolecular isomerism of metal-organic frameworks (MOFs) is known for several structural topologies, having direct implications on the properties of these materials. Although the synthesis of MOF isomers is mainly serendipitous in nature, achieving controlled formation of a target framework is highly relevant for practical applications. This work discusses the influence of additives and synthesis conditions on the formation of porous isomers containing Zn^{2+} as nodes and 2,5-dihydroxy-1,4-benzenedicarboxylate ($dobdc^{4-}$) as linker. Using solvent mixtures containing strongly coordinated molecules, *e.g.* N,N'-dimethylformamide (DMF) and N-methylpyrrolidone (NMP), facilitates the formation of porous structures of type $[Zn_2(dobdc)(S)_x]\cdot yS$ (S = DMF, NMP) which are built from dinuclear $Zn_2(O)_2(CO_2)_3$ secondary building units (SBUs) consisting of two different edge-sharing polyhedrons with the Zn^{2+} ions in a unsaturated coordinative environment. In the presence of water, the

Zn^{2+} dimers are converted to one-dimensional infinite Zn^{2+} chains, in which the number of Zn^{2+}-linker bonds increases, therefore giving a hydrolytically more stable coordination environment. The full characterization of the isomers as well as their conversion to the most stable isomer is presented.

Introduction

Metal-organic frameworks (MOFs) are 3D coordination polymers formed using di- or multitopic organic linkers and metal ions or clusters of metal ions. Currently, more than 20.000 MOF structures are known.[1] The increased focus on the targeted design and tailor-made synthesis of MOFs emerges from their potential applications in gas storage[2–4], molecular separations[3,5,6] and sensing[7–9] as well as catalysis[10–12]. Such broad applications arise from the ability of chemists to fine-tune these materials, even at atomistic level.[13] Tailoring MOF's properties for specific applications can be achieved by making specific topologies[11] and/or introducing key functional groups within the framework.[14] Important parameters in controlling the network topologies are not only the nature of the metal ions and organic linkers used, but also the synthesis parameters, *e.g.* temperature, pressure, reaction time and type of reaction vessel.[13,15] At the same time, the compositional parameters, *i.e.* molar ratio, solvents or solvent mixtures, the addition of modulators, pH and reactants' concentrations also play key roles.[13,15]

The main goal in MOF synthesis is the formation of molecular frameworks in a controlled manner, which is often challenging because of the many synthetic parameters involved. An enticing approach of directing the structure in a controlled manner is to use modulators. The most common type of modulators are coordination modulators that are added in excess directly to the synthesis. They are usually monocarboxylic acids (*e.g.* formic,[16–18] acetic,[16,18–20] benzoic[17,21,22] acids as well as aminoacids[23,24]) which act as competitive coordination agents, regulating the pore size and the morphology of the crystals. Modulators play a key role in the synthesis of Zr-MOFs, facilitating the formation of $Zr_6O_4(OH)_4$ clusters and therefore the growth of the crystals.[22,25] They also slow down the crystal growth rate, therefore avoiding the fast precipitation of amorphous phases.[20,26,27] Kaskel *et al.*[28] reported that the amount of acetic acid used as modulator in the synthesis of $C_{72}H_{36}O_{32}Zr_6$ (DUT-52) has a structure-directing effect because it reduces the connectivity of the $[Zr_6O_4(OH)_4]^{12+}$ entity from 12 to 8 or 6, leading to frameworks with different structural topologies.[28] Modulation can also induce the formation of defects which are responsible for enhanced gas uptake[29,30], proton conduction[31] or catalytic activity.[32–34] Shafir *et al.*,[24] showed that L-proline is an efficient modulator in the synthesis of Zr MOFs with increased particle size.

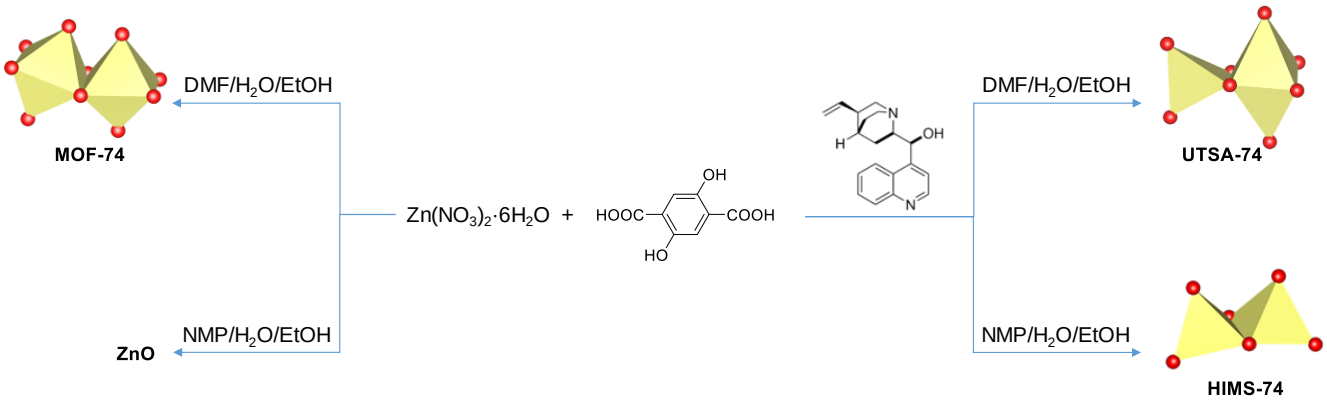

Scheme 1. Influence of the synthetic conditions in the formation of secondary buildings units of porous molecular networks formed from Zn^{2+} as nodes and 2,5-dihydroxy-1,4-benzenedicarboxylate ($dobdc^{4-}$) as linker.

The isostructural metal-organic frameworks known as M-MOF-74[35] are extensively studied due to the presence of unsaturated coordination sites at metal centers,[35,36] their versatility of being prepared with different divalent ions[35] and their high stability at ambient conditions and in the presence of water.[37,38] Among them, Zn-MOF-74 is a very effective material for gas storage[36] and molecular separations[39] and also an active catalyst in several organic transformations[40,41]. Using modulators is not a common approach in the synthesis of MOF-74 series. Only Li *et al.*[42] reported that the size and inherent defects of the nanocrystals of Co-MOF-74 can be tuned by employing salicylic acid as modulator. Our aim was to study the role of *cinchona* alkaloid derivatives, (+)-cinchonine (CN) and (-)-cinchonidine (CD) as coordination modulators in the synthesis of Zn-MOF-74, with the final goal to design chiral frameworks. We hypothesised that the chiral molecules (+)-cinchonine (CN) and (-)-cinchonidine (CD) will coordinate to the Zn^{2+} ions during the crystallisation of Zn-MOF-74, thereby directing the handedness of the molecular framework. Bu *et al.*[43] used *cinchona* alkaloids to prepare a homochiral In^{3+} dicarboxylate framework, $(Me_2NH_2)[In(thb)_2]\cdot x$DMF (known as ATF-1P, H_2thb = thiophene-2,5-dicarboxylic acid), using CD as chiral additive.[44] The chiral alkaloid binds to the In^{3+} ion and directs the handedness of the framework.[44,45] The framework does not belong to a chiral space group due to the racemic distribution of the helical

chains. Based on the structural similarities between the chiral ATF-1P[43] framework with large 1D channels of *ca*. 13 Å[43], which are formed upon interaction with chiral *cinchona* alkaloid modulators, and the MOF-74 framework, which consists of 1D channels of *ca.* 11 Å, we hypothesised that chirality transfer might be achieved upon coordination of CN or CD via amine and hydroxyl groups to the Zn^{2+} ions of MOF-74. Furthermore, the alkaloids can also interact with the framework walls via hydrogen bonding interactions. Indeed, Prochowicz *et al.*[46] reported that *cinchona* alkaloids lead to chiral coordination polymers using noncovalent interaction driven self-assembly processes. However, we found that using *cinchona* alkaloids facilitate the formation of a new Zn-MOF-74 isomer, namely $[Zn_2(dobdc)(NMP)]\cdot$(termed as HIMS-74 in this work), where dobdc is 2,5-dioxido-1,4-benzenedicarboxylate and NMP is N-methylpyrrolidone (Scheme 1). Here, we report the controlled assembly and crystallisation of HIMS-74, and compare its structural features with the previously reported isomers, *e.g.* MOF-74[5] and UTSA-74[5]. The role of the solvent in the stabilisation of specific network topologies is also discussed.

Results and Discussion

Influence of the reaction conditions on the synthesis of MOF-74 isomers

The Zn^{2+} ion in MOF-74 has one coordinatively unsaturated site which is occupied by exchangeable solvent molecule. This site is also available for the coordination of *cinchona* alkaloids molecules. Therefore, we studied the role of both alkaloids and solvent in the hydrothermal reaction of Zn^{2+} with 2,5-dioxido-1,4-benzenedicarboxylic acid (H_2dobdc). Figure 1 shows the alkaloids used in this study.

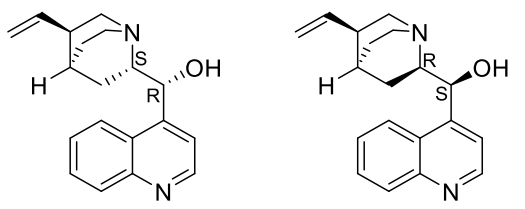

Figure 1. The structure of the *cinchona* alkaloids modulators, indicating the different configurations of the chiral substituted carbon atom centres.

Reacting $Zn(NO_3)_2 \cdot 6H_2O$, H_4dobdc (molar ratio Zn^{2+}:H_4dobdc of 3:1) and CN or CD (1 or 3 equiv.) under hydrothermal conditions in two different solvent mixtures (DMF/EtOH/H_2O or NMP/EtOH/H_2O *v*/*v*/*v* ratio of 20/1/1) afforded six solid crystalline materials. Single-crystal XRD analysis performed on crystals isolated from DMF/EtOH/H_2O reaction mixtures revealed the formation of the compound $[Zn_2(dobdc)(solvent)_2] \cdot xH_2O \cdot yDMF$ (solvent = H_2O or DMF), which crystallises in the rhombohedral $R\underline{3}c$ space group and has a 3D porous structure. The asymmetric unit contains two crystallographically independent Zn^{2+} centres (Zn1 and Zn2) and one $dobdc^{4-}$ linker (Figure 3, left). The Zn1 coordination sphere is composed of four donor atoms from four fully deprotonated linkers, *i.e.* two phenolate oxygens and two carboxylate oxygens, forming a distorted tetrahedral geometry. The Zn1-O bond lengths vary from 1.926(5) to 1.957(5) Å. Zn2 has an octahedral geometry, being surrounded by two phenolate oxygens, two carboxylate oxygens and two oxygen atoms from the solvent molecules (due to the high disorder of the molecular structure, it cannot be determined if the belong to water or DMF molecules. The Zn2-O bond lengths vary from 1.959(5) to 2.120(6) Å. The organic linker binds one Zn^{2+} via carboxylate oxygen O2, while it binds another Zn^{2+} as a chelate via carboxylate O3 and phenolate oxygen O1, forming six-membered rings. All the crystallographic data indicate that this structure is identical with the UTSA-74 structure reported earlier.[5]

Using a polarising optical microscope, the analysis of the solid materials obtained in DMF/EtOH/H_2O solvent mixtures revealed the presence of the chiral alkaloid modulators as aggregates in solution. Therefore, the isolated solid materials were washed thoroughly with the synthesis solvent mixture to fully remove the alkaloids and then all materials were dried at ambient conditions. Notably, the PXRD patterns of these samples matched perfectly the simulated pattern of MOF-74 topology (Figure 2). As indicated by PXRD, the conversion of UTSA-74 to MOF-74 is quantitative and it is most likely caused by the atmospheric humidity due to the prolonged air exposure during the drying process. Indeed, the water induced transformation of UTSA-74 to MOF-74 was also reported by Amelott *et al.*[47]

The formation of UTSA-74 in our work is likely facilitated by the modulating effect of the alkaloids or the DMF/H_2O/EtOH solvent mixture used or perhaps a combination of both. To further test the role of

the alkaloid during the crystallisation process of UTSA-74, we performed the synthesis in the absence of the alkaloid. In this case, however, no solid material was obtained. This result clearly demonstrates that the CN and CD alkaloids play a key role in the formation of the UTSA topology. Furthermore, using XYZ spatial descriptors, we calculated the length of the alkaloids as 11.8 × 9.0 × 7.2 $Å^3$ for CD and 11.8 × 9.3 × 7.3 $Å^3$ for CN. This indicates diffusion restrictions for the alkaloids within the 8.81 Å pores of UTSA-74[48] (Figure S1), thereby explaining the absence of chirality in the isolated molecular structures.

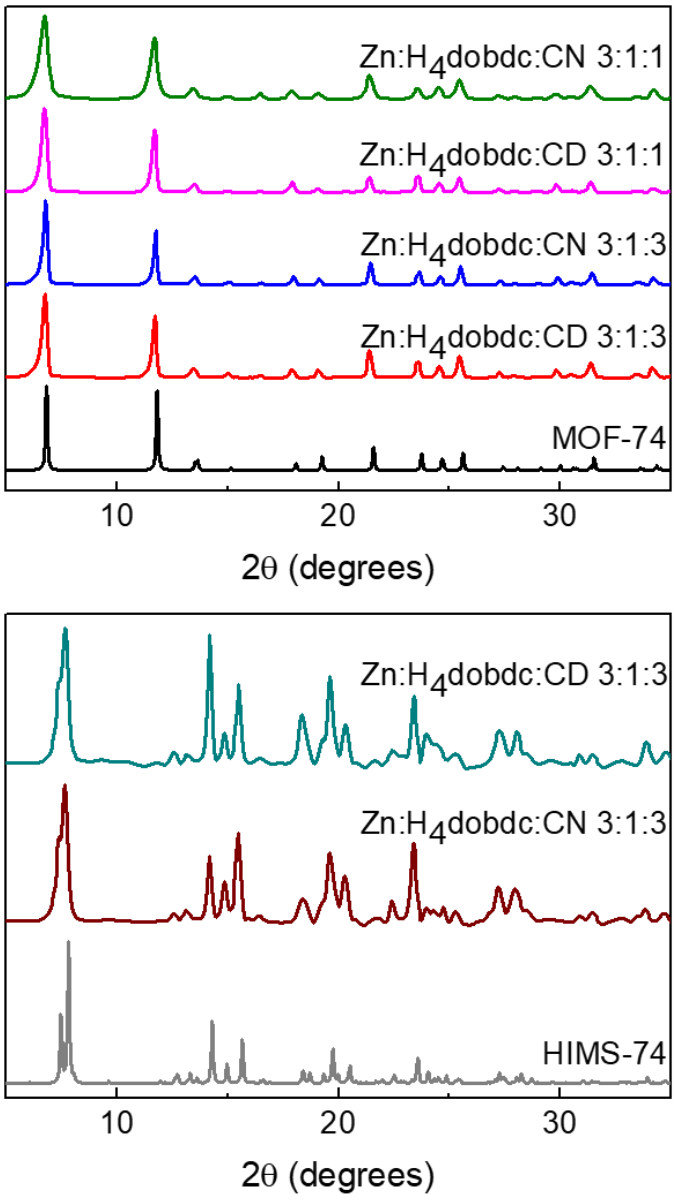

Figure 2. PXRD patterns of the dried materials obtained in DMF (top) and NMP (bottom), and the simulated PXRD patterns for MOF-74[49], UTSA-74 and HIMS-74.

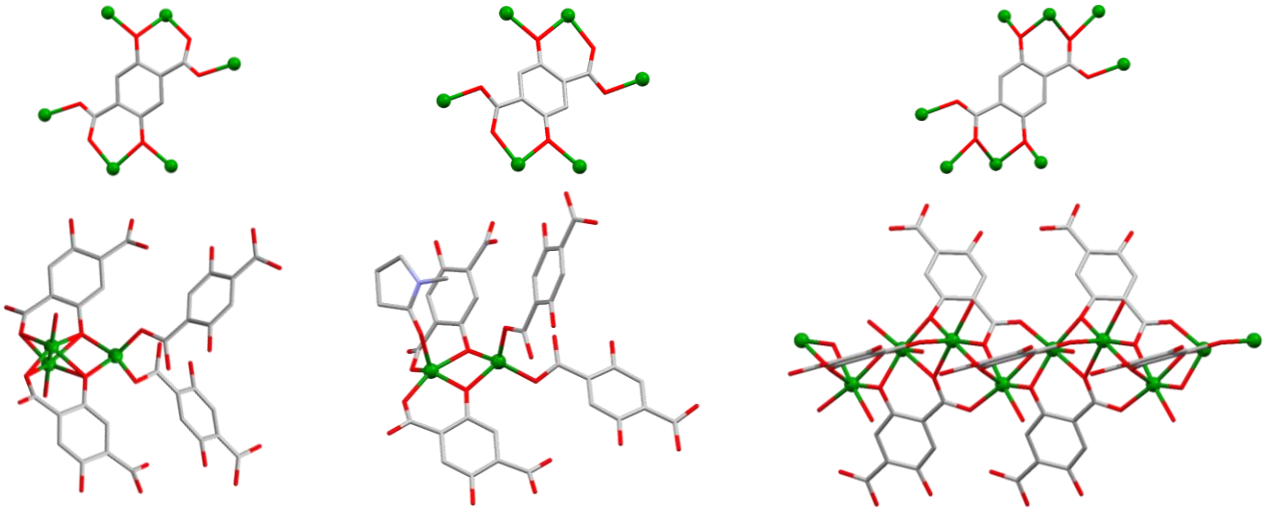

Figure 3. The coordination of $dobdc^{2-}$ to the Zn^{2+} ions and the coordination geometries of the Zn^{2+} ions in UTSA-74 (left), HIMS-74 (middle) and MOF-74[49] (right). The hydrogen atoms and the guest solvent molecules were omitted for clarity. Only the oxygen atom is represented for the disordered coordinated solvent molecules.

Our results show that the unstable UTSA-74 phase forms prior to that of MOF-74 in the presence of *cinchona* alkaloid modulators. Therefore, subsequent studies aimed at understanding the role of the solvent mixture in stabilising the structural topology. We hypothesized that the solvent mixture may also act as a modulator in our synthetic procedure, a phenomenon also frequently reported.[15,50,51] Consequently, we replaced the DMF by the structurally very different *N*-methylpyrrolidone (NMP), which is known to lead to internal shearing stress and formation of a chiral framework, in the case of MOF-5.[52] We envisioned that the $dobdc^{4-}$ linker could exhibit a twisting behaviour upon interaction with the NMP molecules as observed for the benzene-1,4-dicarboxylate linker (bdc^{2-}) in MOF-5. However, replacing DMF with NMP and using a molar ratio of Zn^{2+}:$dobdc^{4-}$:alkaloid equal to 3:1:3 led to a new structural topology, namely $[Zn_2(dobdc)(NMP)]\cdot 0.5(NMP)$ (hereafter denoted as HIMS-74).

HIMS-74 crystallizes in the monoclinic $P2_1/a$ space group. Its asymmetric unit contains two crystallographically independent Zn^{2+} ions. One Zn^{2+} ion is tetracoordinated (Figure 3, middle), being surrounded by two phenolate oxygens and two carboxylate oxygens, forming a distorted tetrahedral

geometry. The Zn-O bond lengths vary between 1.926(3) and 1.970(3) Å. The second Zn^{2+} centre is pentacoordinated, with the coordination sphere defined by two carboxylate oxygens, two phenolate oxygens and the oxygen of the coordinated NMP solvent molecule. The NMP is oriented towards the channels of the framework and its position imposes a distorted square pyramidal geometry. In this case, the Zn-O bond lengths varies from 1.926(3) to 2.092(3) Å. The $dobdc^{4-}$ linkers are hexadentate coordinated, bridging the two independent Zn^{2+} ions via the phenoxo group (Figure 3, middle) whilst the carboxylate groups are bridging Zn^{2+} ions of the same type. The dinuclear $Zn_2(O)_2(CO_2)_3$ secondary building units (SBUs) consist of two edge-sharing polyhedrons which are linked to each other via the carboxylate oxygen donors of the $dobdc^{4-}$ linkers to form a 3D network topology with 1D channels (Figure 4). Notably, the molecular structure of HIMS-74 is built up from dinuclear SBUs as also observed in the case of UTSA-74 and therefore their 3D molecular structures are very similar (Figure 4). The main difference is that the SBUs of HIMS-74 consist of a tetrahedron and a square pyramid whilst the UTSA-74 SBUs are composed of a tetrahedron and an octahedron. This reflects the key role of NMP in stabilising the square pyramidal geometry for the Zn^{2+} ion as compared to DMF which facilitates the stabilisation of the octahedral geometry.

The PXRD patterns (Figure 1, bottom) of the crystalline solids isolated from DMF/H_2O/EtOH solvent mixture shows an excellent matching with the calculated pattern using the single-crystal XRD data of HIMS-74. To understand the role of the alkaloids in the synthesis of HIMS-74, we also performed the synthesis in their absence. Interestingly, the solid materials obtained in these reactions proven to be ZnO, as indicated by PXRD (Figure S3). Moreover, performing the synthesis using one equivalent of alkaloids does not facilitate the formation of the HIMS-74 topology. Therefore, we believe that both the alkaloids and the solvent mixture play key roles in the crystallization process of HIMS-74.

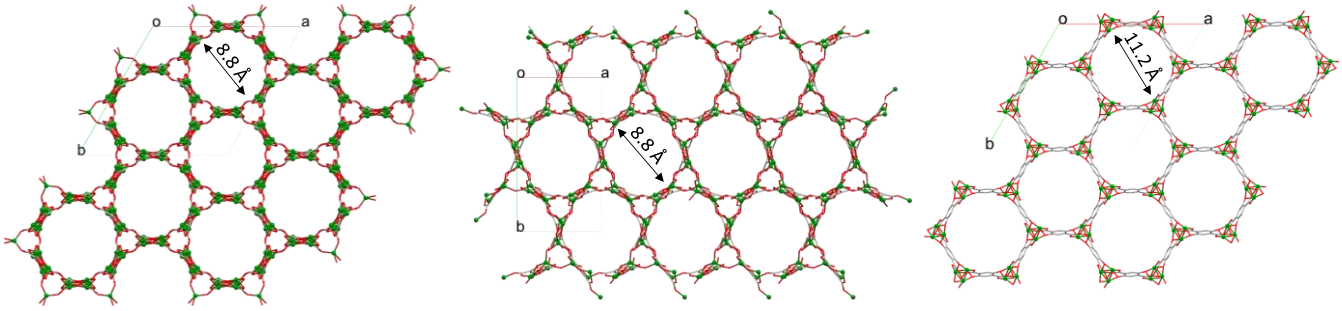

Figure 4. View of the 3D structures of UTSA-74 (left), HIMS-74 (middle) and MOF-74 (right) along the *c* axis. Hydrogen atoms, guest and coordinated solvent molecules are omitted for clarity.

Our studies indicate that some weak interactions between the alkaloids and the SBUs of UTSA-74 and HIMS-74 may favour the formation of dinuclear SBUs as compared to the helical rods present in MOF-74. However, further investigations are necessary to determine the nature of these type of interactions. No induction of chirality using *cinchona* alkaloids as modulators was observed. This suggests that interaction of the alkaloid with the porous framework is weak at best. Under hydrothermal conditions, the alkaloid is easily deprotonated and therefore, can coordinate via its N and O donor atoms (amine and hydroxyl groups) to the Zn^{2+} ions.[46] Therefore, it is likely that the precursors of the HIMS-74 SBUs are doubly bridged dinuclear units (see Figure 5 for details) that prevent the formation of helical rods as observed for MOF-74. The follow up process is the full deprotonation of the hexadentate H_4dobdc linker, which subsequently replaces the *cinchona* alkaloid and forms the HIMS-74 SBUs (Figure 6).

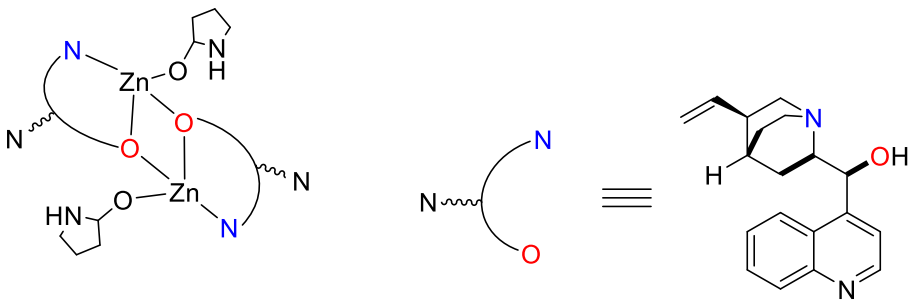

Figure 5. Possible coordination of the c*inchona* alkaloid to the Zn^{2+} ions that precedes the formation of HIMS-74 SBUs.

Phase transformations

As discussed above, the UTSA-74 isomer is not stable and converts to MOF-74 at ambient conditions or in the presence of water. In UTSA-74, there are two types of coordination polyhedrons for Zn^{2+} ions, tetrahedron and octahedron, whilst both Zn^{2+} ions have an octahedral geometry in MOF-74. The SBUs of UTSA-74 consist of $Zn_2(O)_2(CO_2)_4$ units connected by chains of $dobdc^{4-}$ linkers.[47] MOF-74 contains helical chains of edge-sharing ZnO_6 octahedra that are interconnected via $dobdc^{4-}$ linkers.[49] Ameloot *et al.*[47] attributed the formation of the discrete SBUs in UTSA-74 to a stabilising effect of the DMSO solvent. However, Chen *et al.*[5] synthesised UTSA-74 in DMF/H_2O, a similar solvent mixture used for preparing MOF-74.[49] Our studies show that both the solvent mixture (DMF/H_2O/EtOH) as well as the c*inchona* alkaloids play key role in the formation of UTSA-74. All these results indicate that the formation of the UTSA-74 framework is very complex and depends on many more factors, including the anions present in the reaction mixture (*e.g.* CH_3COO^-)[47] as well as the temperature and reaction time (*e.g.* 72 hours).[47]

As proposed by Ameloot *et al.*,[47] it is important to consider the potential formation of UTSA-74 topology in the nucleation and growth process of MOF-74. This implies to consider a sequential stepwise model, known as Ostwald's Rule of Stages,[53] rather than a classical nucleation and growth model. A careful selection of the reaction parameters and an in-depth morphological analysis of the single crystals formed are required to understand a such complex phase transition. The Zn-UTSA-74 single crystals can be easily distinguished from those of Zn-MOF-74 by analysing their morphology using polarised light microscopy. Initial studies reported that the Zn-UTSA-74 crystallises as yellow rod crystals[5], but also hexagonal[47] crystals were observed. *In situ* PXRD and SEM analysis of the Zn-UTSA-74 to Zn-MOF-74 phase transitions have shown that the nucleation and growth of the Zn-MOF-74 occurs at the surface of hexagonally shaped UTSA-74 crystals.[47] This indicates that the MOF-74 phase is thermodynamically more stable. The conversion of the Zn^{2+} dimers of UTSA-74 to the one-dimensional infinite Zn^{2+} chains in MOF-74 increases the number of Zn^{2+}-linker bonds from four to five, giving a hydrolytically more stable coordination environment.[47]

HIMS-74 is a highly stable topology at ambient conditions and it does not undergo any structural changes. Attempts to replace the strongly coordinated NMP molecules have revealed that exposing HIMS-74 to polar organic solvents (*e.g.* CH_3OH) leads to a loss in crystallinity and partial or complete transition to UTSA-74 is likely to occur (Figure S6). SEM analysis taken after immersion of HIMS-74 in CH_3OH (6 days) indicate that the morphology is no longer homogeneous and a wide distribution of crystal size is obtained (Figure S7). TGA-DSC analysis on the recovered sample also showed that no NMP solvent was present (Figure S8) and N_2 adsorption studies indicated the lack of porosity in this material. The integrity of the HIMS-74 topology is retained in acetone (Figure S6), however NMP is not replaced in the sample as shown in the TGA-DSC analysis (Figure S8). To further test the stability of HIMS-74 in water, the solid crystalline material was immersed in water for 20 h. PXRD and SEM studies indicates that HIMS-74 is converted to MOF-74 (Figure S9-S10). These results show HIMS-74 also undergoes a water-mediated isomerization to MOF-74 and possibly UTSA-74, but the HIMS-74 to MOF-74 phase transition is faster than that of HIMS-74 to UTSA-74 (Figure S9).

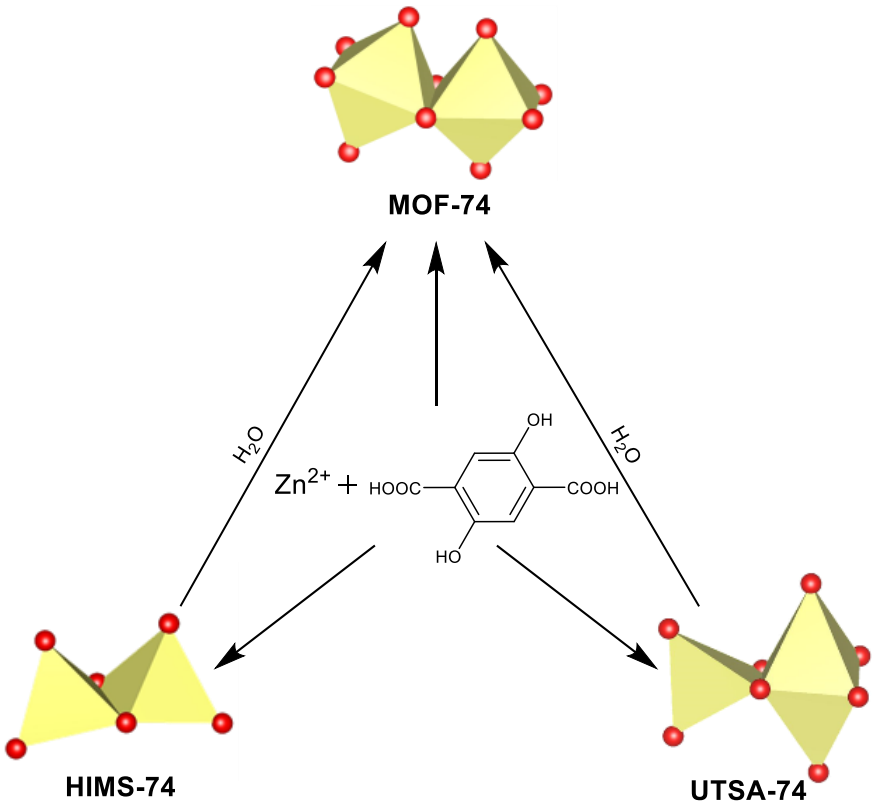

Figure 6. Role of the synthetic conditions in the synthesis of MOF-74 isomers.

Unlike UTSA-74, HIMS-74 is stable upon separation from the mother liquor and drying in air, indicating that NMP has a stabilizing effect due to its strong coordination to the Zn^{2+} ions. Moreover, the close orientation of the coordinated NMP molecules towards the aromatic linkers in the single-crystal XRD analysis indicates a bonding via CH···π interactions (*ca.* 3.2 Å). One non-coordinated NMP molecule is also in close contact with the coordinated NMP and it interacts via moderate hydrogen bonding through the carbonyl O atoms, with a CH···O bond distance of 2.6-2.8 Å. Earlier studies[52,54] also showed that the molecular size and the chemical nature of NMP give rise to structural transformation, *e.g.* chiral transformation in MOF-5.

MOF-74 is intensely studied for gas storage,[55,56] molecular separations[57] and catalysis applications.[58,59] Notably, MOF-74 also shows a very high CO_2 uptake due to the presence of three different CO_2 adsorption sites.[60] The first one is based on the electrostatic interaction between the open metal site and CO_2, the second one is related to the van der Waals interaction of the CO_2 with the host framework, and the third is only related to the filling of the MOF channels. Although UTSA-74 has the same number of open metal sites per SBU as MOF-74, a smaller CO_2 uptake was observed for UTSA-74 (90 cm^3/cm^3) as compared to MOF-74 (146 cm^3/cm^3).[5] This was ascribed due to the loose packing of the CO_2 molecules in UTSA-74 (7.5 Å O···O) as compared to MOF-74 (3.6 Å O···O)[5], and also to the slightly smaller pores size. The available open sites in HIMS-74 indicate two adsorption sites per SBU unit, similar to UTSA-74, and therefore similar CO_2 uptake is expected. Nevertheless, we have not been able to verify it experimentally because both N_2 and CO_2 adsorption studies indicated that HIMS-74 is not porous. This is due to the unsuccessful removal of the coordinated NMP molecules without loss of crystallinity and it clearly demonstrates the key role of NMP in stabilizing the HIMS-74 framework.

Conclusions

This work demonstrates that the designed synthesis of MOFs remains a complex process and that the starting materials, synthesis solvents and the modulators play critical role in the stabilisation of various network topologies. Specifically, we showed that using c*inchona* alkaloids as modulators as well as the

choice of solvent have direct implications for the crystallisation of different MOF-74 isomers. In addition to the previously known MOF-74 and UTSA-74 frameworks, a new HIMS-74 topology is formed when using NMP instead of DMF as coordinating solvent molecules. Unlike UTSA-74, HIMS-74 isomer is more stable at ambient conditions and it undergoes a solvent-mediated isomerisation to MOF-74 only by immersing it in water. A comparative study of the adsorption properties of the three isomers was not possible because HIMS-74 topology is not stable upon solvent removal. This work highlights a new strategy to control the framework topology when using Zn^{2+} nodes and $dobdc^{4-}$ linkers. It can also be applied to other MOF systems, thus affording the facile synthesis of structural isomers that enable structure-property correlations.

Supporting Information

The Supporting Information is available free of charge on the ACS Publications website at DOI: xx.xxxx/acs.inorgchem.xxxxxx. It includes TGA, PXRD, SEM and porosity studies. Structural information was deposited at the Cambridge Crystallographic Data Center and it may be obtained free of charge from The Director, CCDC, 12 Union Road, Cambridge CB2 1EZ, UK (fax +44 1223 366 033); e-mail: deposit@ccdc.cam.ac.uk or http://www.ccdc.cam.ac.uk) (CCDC reference nos. 1884101 for HIMS-74 and 1884102 for UTSA-74.

Corresponding author

*E-mail: s.grecea@uva.nl (S. Tanase)

ORCID?

Notes

The authors declare no competing financial interest.

Author Contributions

The manuscript was written through contributions of all authors. All authors have given approval to the final version of the manuscript.

Experimental Section

Materials

All chemicals were purchased from commercial suppliers and used without further purification. The bulk synthesis of UTSA-74 used for the phase transition studies was performed following a reported procedure.[47] The MOF-74 sample for SEM studies was prepared using a procedure from literature.[61]

Synthesis of $[Zn_2(dobdc)(DMF)_2]\cdot xH_2O\cdot y$DMF (UTSA-74)

A mixture of $Zn(NO_3)_2\cdot 6H_2O$ (0.089 g, 0.3 mmol), 2,5-dihydroxyterephthalic acid (0.019 g, 0.1 mmol), (-)-cinchonidine alkaloid (0.088 g, 0.3 mmol) and a solvent mixture of DMF:H_2O:EtOH (20:1:1 v:v:v, 15 mL) was placed in a 20-mL Teflon screw-capped DuranTM Pyrex tube. The mixture was sonicated, then placed in a preheated oven at 120 °C and kept for 48 h. The reaction mixture was then cooled down to room temperature and the solid crystalline material was filtered and washed three times with the synthesis solvent. IR (KBr, cm^{-1}): 3434 (m, b), 2959 (w), 2927 (w), 1656 (s, s), 1559 (s, s), 1511 (w), 1450 (m, s), 1410 (s, s), 1363 (w), 1307 (w), 1239 (m, s), 1196 (m, s), 1114 (w, s), 1063 (w), 910 (w), 879 (m, s), 815 (m, s), 676 (w), 635 (w), 578 (w, s).

Synthesis of $[Zn_2(dobdc)(NMP)]\cdot 0.5$NMP (HIMS-74)

A mixture of $Zn(NO_3)_2\cdot 6H_2O$ (0.089 g, 0.3 mmol), 2,5-dihydroxyterephthalic acid (0.019 g, 0.1 mmol), (-)-cinchonidine alkaloid (0.088 g, 0.3 mmol) and a solvent mixture of NMP:H_2O:EtOH (20:1:1 v:v:v, 15 mL) was placed in a 20-mL Teflon screw-capped DuranTM Pyrex tube. The mixture was sonicated, then placed in a preheated oven at 120 °C and kept for 48 h. The reaction mixture was then cooled down to room temperature and the solid crystalline material was filtered and washed three times with NMP and one time with acetone. IR (KBr, cm^{-1}): 3436 (m, b), 2958 (w), 2927 (w), 2873 (w), 1662 (m, s), 1646 (m, s), 1535 (s, s), 1469 (m, s), 1434 (m, s), 1410 (m, s), 1383 (m, b), 1304 (w, b), 1256 (m, s), 1234 (m, s), 1214 (m, s), 1119 (w, b), 1031 (w), 990 (w), 891 (m, s), 825 (m, s), 802 (m, s), 670 (w), 610 (m, s). C, H,

N analysis (%): calcd. for $[Zn_2(dobdc)(NMP)]\cdot 0.5(NMP)$ ($Zn_2C_{15.5}H_{15.5}N_{1.5}O_{7.5}$) C 39.31, H 3.31, N 4.44; found C 38.72, H 3.54, N 4.14.

Physical characterisation

Powder X-ray diffraction (PXRD) measurements were carried out from 3° to 60° at 2° min^{-1} speed rate using a Rigaku Miniflex X-ray Diffractometer. The PDF Card No. 2300112 was used as reference for the PRXD of ZnO. Thermogravimetric analysis (TGA) and differential scanning calorimetry (DSC) were performed in the 35-800 °C range at 5 $K\cdot min^{-1}$ using a NETZSCH Jupiter ® STA 449F3 instrument. The measurements were carried out under flow of argon (20 $mL\cdot min^{-1}$) and protective argon (20 $mL\cdot min^{-1}$). N_2 and CO_2 adsorption isotherms were measured on a Thermo Scientific Surfer instrument at 77 K and 273K, respectively. The solvent exchanged UTSA-74 sample was activated following the procedures from literature[47]. The as synthesised HIMS-74 was pretreated in vacuum with 2 °/min heating from room temperature to 100 °C and a hold of 1h, and from 100 °C to 250 °C with a hold of 6h. Another activation procedure was vacuum heating with a ramp of 4 °/min from room temperature to 200 °C and a hold of 2h. The methanol exchanged HIMS-74 sample was heated under vacuum from room temperature to 80 °C with a ramp of 2 °/min and 1h hold, then heating to 120 °C with 4 °/min and 1h hold, and lastly to 220 °C with 2 °/min and a final hold of 12h. Scanning electron micrographs were obtained by using a field emission scanning electron microscope FEI-Verios 460. The samples were previously sputtered with a 20 mm thick Au layer using the Leica EM ACE600 Double sputter coater.

Single-Crystal X-Ray Diffraction (SCXRD) data of HIMS-74 and UTSA-74 analogue were collected at 100(2) K in BL13-XALOC beamline[62] at the ALBA synchrotron, on a single-axis goniometer with a Pilatus 6M detector using a monochromatic X-ray beam ($\lambda = 0.82656$ Å). The data frames were integrated and scaled using XDS software packakge.[63] Absorption correction was not applied. The structure was solved by direct methods and subsequently refined by correction of F2 against all reflections, using SHELXT2013 and SHELXL2013 within the WinGX package.[64–66] Both structures contains some

disorder molecules. Attempts to adequately model the disordered molecules were unsatisfactory; therefore, the PLATON/SQUEEZE routine was applied to mask out the disordered electron density.[67]

Acknowledgements

This work is part of the Research Priority Area Sustainable Chemistry of the University of Amsterdam, http://suschem.uva.nl, and was funded by a TOP-PUNT grant from NWO. It was also supported by the Spanish MINECO (projects PN MAT2015-65354-C2-1-R), the Catalan AGAUR (project 2014 SGR 80), the ERC under the EU-FP7 (ERC-Co 615954), and the CERCA Program/Generalitat de Catalunya. ICN2 is supported by the Severo Ochoa program from Spanish MINECO (Grant No. SEV-2017-0706). The authors would like to thank Thierry Slot for his assistance in SEM measurements.

References

(1) Furukawa, H.; Cordova, K. E.; O'Keeffe, M.; Yaghi, O. M. The Chemistry and Applications of Metal-Organic Frameworks. *Science* **2013**, *341* (6149), 1230444. https://doi.org/10.1126/science.1230444.

(2) Bao, Z.; Yu, L.; Ren, Q.; Lu, X.; Deng, S. Adsorption of CO2 and CH4 on a Magnesium-Based Metal Organic Framework. *J. Colloid Interface Sci.* **2011**, *353* (2), 549–556. https://doi.org/10.1016/j.jcis.2010.09.065.

(3) Adhikari, A. K.; Lin, K.-S. Improving CO2 Adsorption Capacities and CO2/N2 Separation Efficiencies of MOF-74(Ni, Co) by Doping Palladium-Containing Activated Carbon. *Chem. Eng. J.* **2016**, *284*, 1348–1360. https://doi.org/10.1016/j.cej.2015.09.086.

(4) Sillar, K.; Hofmann, A.; Sauer, J. Ab Initio Study of Hydrogen Adsorption in MOF-5. *J. Am. Chem. Soc.* **2009**, *131* (11), 4143–4150. https://doi.org/10.1021/ja8099079.

(5) Luo, F.; Yan, C.; Dang, L.; Krishna, R.; Zhou, W.; Wu, H.; Dong, X.; Han, Y.; Hu, T.-L.; O'Keeffe, M.; et al. UTSA-74: A MOF-74 Isomer with Two Accessible Binding Sites per Metal Center for Highly Selective Gas Separation. *J. Am. Chem. Soc.* **2016**, *138* (17), 5678–5684. https://doi.org/10.1021/jacs.6b02030.

(6) Fu, J.; Das, S.; Xing, G.; Ben, T.; Valtchev, V.; Qiu, S. Fabrication of COF-MOF Composite Membranes and Their Highly Selective Separation of H2/CO2. *J. Am. Chem. Soc.* **2016**, *138* (24), 7673–7680. https://doi.org/10.1021/jacs.6b03348.

(7) Song, X.-Z.; Meng, Y.-L.; Tan, Z.; Qiao, L.; Huang, T.; Wang, X.-F. Concave ZnFe2O4 Hollow Octahedral Nanocages Derived from Fe-Doped MOF-5 for High-Performance Acetone Sensing at Low-Energy Consumption. *Inorg. Chem.* **2017**, *56* (22), 13646–13650. https://doi.org/10.1021/acs.inorgchem.7b02425.

(8) Bhardwaj, N.; Bhardwaj, S. K.; Mehta, J.; Kim, K.-H.; Deep, A. MOF–Bacteriophage Biosensor for Highly Sensitive and Specific Detection of Staphylococcus Aureus. *ACS Appl. Mater. Interfaces* **2017**, *9* (39), 33589–33598. https://doi.org/10.1021/acsami.7b07818.

(9) Freund, P.; Senkovska, I.; Kaskel, S. Switchable Conductive MOF–Nanocarbon Composite Coatings as Threshold Sensing Architectures. *ACS Appl. Mater. Interfaces* **2017**, *9* (50), 43782–43789. https://doi.org/10.1021/acsami.7b13924.
(10) Stubbs, A. W.; Braglia, L.; Borfecchia, E.; Meyer, R. J.; Román- Leshkov, Y.; Lamberti, C.; Dincă, M. Selective Catalytic Olefin Epoxidation with MnII-Exchanged MOF-5. *ACS Catal.* **2018**, *8* (1), 596–601. https://doi.org/10.1021/acscatal.7b02946.
(11) Deria, P.; Gómez-Gualdrón, D. A.; Hod, I.; Snurr, R. Q.; Hupp, J. T.; Farha, O. K. Framework-Topology-Dependent Catalytic Activity of Zirconium-Based (Porphinato)zinc(II) MOFs. *J. Am. Chem. Soc.* **2016**, *138* (43), 14449–14457. https://doi.org/10.1021/jacs.6b09113.
(12) Song, J.; Zhang, Z.; Hu, S.; Wu, T.; Jiang, T.; Han, B. MOF-5/N-Bu4NBr: An Efficient Catalyst System for the Synthesis of Cyclic Carbonates from Epoxides and CO2 under Mild Conditions. *Green Chem.* **2009**, *11* (7), 1031–1036. https://doi.org/10.1039/B902550B.
(13) Stock, N.; Biswas, S. Synthesis of Metal-Organic Frameworks (MOFs): Routes to Various MOF Topologies, Morphologies, and Composites. *Chem. Rev.* **2012**, *112* (2), 933–969. https://doi.org/10.1021/cr200304e.
(14) Liu, L.; Zhou, T.-Y.; Telfer, S. G. Modulating the Performance of an Asymmetric Organocatalyst by Tuning Its Spatial Environment in a Metal–Organic Framework. *J. Am. Chem. Soc.* **2017**. https://doi.org/10.1021/jacs.7b07921.
(15) Seetharaj, R.; Vandana, P. V.; Arya, P.; Mathew, S. Dependence of Solvents, pH, Molar Ratio and Temperature in Tuning Metal Organic Framework Architecture. *Arab. J. Chem.* **in press**. https://doi.org/10.1016/j.arabjc.2016.01.003.
(16) Hu, Z.; Castano, I.; Wang, S.; Wang, Y.; Peng, Y.; Qian, Y.; Chi, C.; Wang, X.; Zhao, D. Modulator Effects on the Water-Based Synthesis of Zr/Hf Metal–Organic Frameworks: Quantitative Relationship Studies between Modulator, Synthetic Condition, and Performance. *Cryst. Growth Des.* **2016**, *16* (4), 2295–2301. https://doi.org/10.1021/acs.cgd.6b00076.
(17) Bumstead, A. M.; Cordes, D. B.; Dawson, D. M.; Chakarova, K. K.; Mihaylov, M. Y.; Hobday, C. L.; Düren, T.; Hadjiivanov, K. I.; Slawin, A. M. Z.; Ashbrook, S. E.; et al. Modulator-Controlled Synthesis of Microporous STA-26, an Interpenetrated 8,3-Connected Zirconium MOF with the the-I Topology, and Its Reversible Lattice Shift. *Chem. – Eur. J.* **2018**, *24* (23), 6115–6126. https://doi.org/10.1002/chem.201705136.
(18) Bagherzadeh, E.; Zebarjad, S. M.; Hosseini, H. R. M. Morphology Modification of the Iron Fumarate MIL-88A Metal-Organic Framework Using Formic Acid and Acetic Acid as Modulators. *Eur. J. Inorg. Chem.* **2018**, No. 18, 1909–1915. https://doi.org/10.1002/ejic.201800056.
(19) Bon, V.; Senkovska, I.; Baburin, I. A.; Kaskel, S. Zr- and Hf-Based Metal–Organic Frameworks: Tracking Down the Polymorphism. *Cryst. Growth Des.* **2013**, *13* (3), 1231–1237. https://doi.org/10.1021/cg301691d.
(20) Tsuruoka, T.; Furukawa, S.; Takashima, Y.; Yoshida, K.; Isoda, S.; Kitagawa, S. Nanoporous Nanorods Fabricated by Coordination Modulation and Oriented Attachment Growth. *Angew. Chem.* **2009**, *121* (26), 4833–4837. https://doi.org/10.1002/ange.200901177.
(21) Schaate, A.; Roy, P.; Preuße, T.; Lohmeier, S. J.; Godt, A.; Behrens, P. Porous Interpenetrated Zirconium–Organic Frameworks (PIZOFs): A Chemically Versatile Family of Metal–Organic Frameworks. *Chem. – Eur. J.* **2011**, *17* (34), 9320–9325. https://doi.org/10.1002/chem.201101015.
(22) Schaate, A.; Roy, P.; Godt, A.; Lippke, J.; Waltz, F.; Wiebcke, M.; Behrens, P. Modulated Synthesis of Zr-Based Metal–Organic Frameworks: From Nano to Single Crystals. *Chem. – Eur. J.* **2011**, *17* (24), 6643–6651. https://doi.org/10.1002/chem.201003211.
(23) Marshall, R. J.; Hobday, C. L.; Murphie, C. F.; Griffin, S. L.; Morrison, C. A.; Moggach, S. A.; Forgan, R. S. Amino Acids as Highly Efficient Modulators for Single Crystals of Zirconium and Hafnium Metal-Organic Frameworks. *J. Mater. Chem. A* **2016**, *4* (18), 6955–6963. https://doi.org/10.1039/c5ta10401g.
(24) Gutov, O. V.; Molina, S.; Escudero- Adán, E. C.; Shafir, A. Modulation by Amino Acids: Toward Superior Control in the Synthesis of Zirconium Metal–Organic Frameworks. *Chem. – Eur. J. 22* (38), 13582–13587. https://doi.org/10.1002/chem.201600898.

(25) Katz, M. J.; Brown, Z. J.; Colón, Y. J.; Siu, P. W.; Scheidt, K. A.; Snurr, R. Q.; Hupp, J. T.; Farha, O. K. A Facile Synthesis of UiO-66, UiO-67 and Their Derivatives. *Chem. Commun.* **2013**, *49* (82), 9449–9451. https://doi.org/10.1039/C3CC46105J.
(26) Diring, S.; Furukawa, S.; Takashima, Y.; Tsuruoka, T.; Kitagawa, S. Controlled Multiscale Synthesis of Porous Coordination Polymer in Nano/Micro Regimes. *Chem. Mater.* **2010**, *22* (16), 4531–4538. https://doi.org/10.1021/cm101778g.
(27) Zahn, G.; Zerner, P.; Lippke, J.; Kempf, F. L.; Lilienthal, S.; Schröder, C. A.; Schneider, A. M.; Behrens, P. Insight into the Mechanism of Modulated Syntheses: In Situ Synchrotron Diffraction Studies on the Formation of Zr-Fumarate MOF. *CrystEngComm* **2014**, *16* (39), 9198–9207. https://doi.org/10.1039/C4CE01095G.
(28) Bon, V.; Senkovska, I.; Weiss, M. S.; Kaskel, S. Tailoring of Network Dimensionality and Porosity Adjustment in Zr- and Hf-Based MOFs. *CrystEngComm* **2013**, *15* (45), 9572–9577. https://doi.org/10.1039/C3CE41121D.
(29) Wu, H.; Chua, Y. S.; Krungleviciute, V.; Tyagi, M.; Chen, P.; Yildirim, T.; Zhou, W. Unusual and Highly Tunable Missing-Linker Defects in Zirconium Metal–Organic Framework UiO-66 and Their Important Effects on Gas Adsorption. *J. Am. Chem. Soc.* **2013**, *135* (28), 10525–10532. https://doi.org/10.1021/ja404514r.
(30) Liang, W.; Coghlan, C. J.; Ragon, F.; Rubio-Martinez, M.; D'Alessandro, D. M.; Babarao, R. Defect Engineering of UiO-66 for CO2 and H2O Uptake – a Combined Experimental and Simulation Study. *Dalton Trans.* **2016**, *45* (11), 4496–4500. https://doi.org/10.1039/C6DT00189K.
(31) Taylor, J. M.; Dekura, S.; Ikeda, R.; Kitagawa, H. Defect Control To Enhance Proton Conductivity in a Metal–Organic Framework. *Chem. Mater.* **2015**, *27* (7), 2286–2289. https://doi.org/10.1021/acs.chemmater.5b00665.
(32) Gutov, O. V.; Hevia, M. G.; Escudero-Adán, E. C.; Shafir, A. Metal–Organic Framework (MOF) Defects under Control: Insights into the Missing Linker Sites and Their Implication in the Reactivity of Zirconium-Based Frameworks. *Inorg. Chem.* **2015**, *54* (17), 8396–8400. https://doi.org/10.1021/acs.inorgchem.5b01053.
(33) Vermoortele, F.; Bueken, B.; Le Bars, G.; Van de Voorde, B.; Vandichel, M.; Houthoofd, K.; Vimont, A.; Daturi, M.; Waroquier, M.; Van Speybroeck, V.; et al. Synthesis Modulation as a Tool To Increase the Catalytic Activity of Metal–Organic Frameworks: The Unique Case of UiO-66(Zr). *J. Am. Chem. Soc.* **2013**, *135* (31), 11465–11468. https://doi.org/10.1021/ja405078u.
(34) Canivet, J.; Vandichel, M.; Farrusseng, D. Origin of Highly Active Metal–organic Framework Catalysts: Defects? Defects! *Dalton Trans.* **2016**, *45* (10), 4090–4099. https://doi.org/10.1039/C5DT03522H.
(35) Rosnes, M. H.; Opitz, M.; Frontzek, M.; Lohstroh, W.; Embs, J. P.; Georgiev, P. A.; Dietzel, P. D. C. Intriguing Differences in Hydrogen Adsorption in CPO-27 Materials Induced by Metal Substitution. *J. Mater. Chem. A* **2015**, *3* (9), 4827–4839. https://doi.org/10.1039/C4TA05794E.
(36) Wu, H.; Zhou, W.; Yildirim, T. High-Capacity Methane Storage in Metal−Organic Frameworks M2(dhtp): The Important Role of Open Metal Sites. *J. Am. Chem. Soc.* **2009**, *131* (13), 4995–5000. https://doi.org/10.1021/ja900258t.
(37) Kizzie, A. C.; Wong-Foy, A. G.; Matzger, A. J. Effect of Humidity on the Performance of Microporous Coordination Polymers as Adsorbents for CO2 Capture. *Langmuir* **2011**, *27* (10), 6368–6373. https://doi.org/10.1021/la200547k.
(38) Liu, J.; Benin, A. I.; Furtado, A. M. B.; Jakubczak, P.; Willis, R. R.; LeVan, M. D. Stability Effects on CO2 Adsorption for the DOBDC Series of Metal–Organic Frameworks. *Langmuir* **2011**, *27* (18), 11451–11456. https://doi.org/10.1021/la201774x.
(39) Caskey, S. R.; Wong-Foy, A. G.; Matzger, A. J. Dramatic Tuning of Carbon Dioxide Uptake via Metal Substitution in a Coordination Polymer with Cylindrical Pores. *J. Am. Chem. Soc.* **2008**, *130* (33), 10870–10871. https://doi.org/10.1021/ja8036096.
(40) Srinivas, G.; Ford, J.; Zhou, W.; Yildirim, T. Zn-MOF Assisted Dehydrogenation of Ammonia Borane: Enhanced Kinetics and Clean Hydrogen Generation. *Int. J. Hydrog. Energy* **2012**, *37* (4), 3633–3638. https://doi.org/10.1016/j.ijhydene.2011.04.008.

(41) Botas, J. A.; Calleja, G.; Sánchez-Sánchez, M.; Orcajo, M. G. Effect of Zn/Co Ratio in MOF-74 Type Materials Containing Exposed Metal Sites on Their Hydrogen Adsorption Behaviour and on Their Band Gap Energy. *Int. J. Hydrog. Energy* **2011**, *36* (17), 10834–10844. https://doi.org/10.1016/j.ijhydene.2011.05.187.
(42) Yan, W.; Guo, Z.; Xu, H.; Lou, Y.; Chen, J.; Li, Q. Downsizing Metal–organic Frameworks with Distinct Morphologies as Cathode Materials for High-Capacity Li–O2 Batteries. *Mater. Chem. Front.* **2017**, *1* (7), 1324–1330. https://doi.org/10.1039/C6QM00338A.
(43) Zhang, J.; Chen, S.; Wu, T.; Feng, P.; Bu, X. Homochiral Crystallization of Microporous Framework Materials from Achiral Precursors by Chiral Catalysis. *J. Am. Chem. Soc.* **2008**, *130* (39), 12882–12883. https://doi.org/10.1021/ja805272j.
(44) Morris, R. E.; Bu, X. Induction of Chiral Porous Solids Containing Only Achiral Building Blocks. *Nat. Chem.* **2010**, *2* (5), 353–361. https://doi.org/10.1038/nchem.628.
(45) Kaczorowski, T.; Justyniak, I.; Lipińska, T.; Lipkowski, J.; Lewiński, J. Metal Complexes of Cinchonine as Chiral Building Blocks: A Strategy for the Construction of Nanotubular Architectures and Helical Coordination Polymers. *J. Am. Chem. Soc.* **2009**, *131* (15), 5393–5395. https://doi.org/10.1021/ja8098867.
(46) Lewiński, J.; Kaczorowski, T.; Justyniak, I.; Prochowicz, D. Development of Chiral N,N-Ditopic Metalloligands Based on a Cinchona Alkaloids' Backbone for Constructing Homochiral Coordination Polymers. *Chem. Commun.* **2010**, *47* (3), 950–952. https://doi.org/10.1039/C0CC03586F.
(47) Bueken, B.; Reinsch, H.; Heidenreich, N.; Vandekerkhove, A.; Vermoortele, F.; Kirschhock, C. E. A.; Stock, N.; Vos, D. D.; Ameloot, R. An in Situ Investigation of the Water-Induced Phase Transformation of UTSA-74 to MOF-74(Zn). *CrystEngComm* **2017**, *19* (29), 4152–4156. https://doi.org/10.1039/C7CE00094D.
(48) Dubbeldam, D.; Calero, S.; Vlugt, T. J. H. iRASPA: GPU-Accelerated Visualization Software for Materials Scientists. *Mol. Simul.* **2018**, *44* (8), 653–676. https://doi.org/10.1080/08927022.2018.1426855.
(49) Rosi, N. L.; Kim, J.; Eddaoudi, M.; Chen, B.; O'Keeffe, M.; Yaghi, O. M. Rod Packings and Metal−Organic Frameworks Constructed from Rod-Shaped Secondary Building Units. *J. Am. Chem. Soc.* **2005**, *127* (5), 1504–1518. https://doi.org/10.1021/ja045123o.
(50) Li, C.-P.; Du, M. Role of Solvents in Coordination Supramolecular Systems. *Chem. Commun.* **2011**, *47* (21), 5958–5972. https://doi.org/10.1039/C1CC10935A.
(51) Zhou, X.; Liu, P.; Huang, W.-H.; Kang, M.; Wang, Y.-Y.; Shi, Q.-Z. Solvents Influence on Sizes of Channels in Three Fry Topological Mn(II)-MOFs Based on Metal–carboxylate Chains: Syntheses, Structures and Magnetic Properties. *CrystEngComm* **2013**, *15* (40), 8125–8132. https://doi.org/10.1039/C3CE41120F.
(52) Evans, J. D.; Coudert, F.-X. Microscopic Mechanism of Chiral Induction in a Metal–Organic Framework. *J. Am. Chem. Soc.* **2016**, *138* (19), 6131–6134. https://doi.org/10.1021/jacs.6b02781.
(53) Van Vleet, M. J.; Weng, T.; Li, X.; Schmidt, J. R. In Situ, Time-Resolved, and Mechanistic Studies of Metal–Organic Framework Nucleation and Growth. *Chem. Rev.* **2018**, *118* (7), 3681–3721. https://doi.org/10.1021/acs.chemrev.7b00582.
(54) Zhang, S.-Y.; Li, D.; Guo, D.; Zhang, H.; Shi, W.; Cheng, P.; Wojtas, L.; Zaworotko, M. J. Synthesis of a Chiral Crystal Form of MOF-5, CMOF-5, by Chiral Induction. *J. Am. Chem. Soc.* **2015**, *137* (49), 15406–15409. https://doi.org/10.1021/jacs.5b11150.
(55) Mason, J. A.; Veenstra, M.; Long, J. R. Evaluating Metal–organic Frameworks for Natural Gas Storage. *Chem Sci* **2014**, *5* (1), 32–51. https://doi.org/10.1039/C3SC52633J.
(56) Liu, Y.; Kabbour, H.; Brown, C. M.; Neumann, D. A.; Ahn, C. C. Increasing the Density of Adsorbed Hydrogen with Coordinatively Unsaturated Metal Centers in Metal−Organic Frameworks. *Langmuir* **2008**, *24* (9), 4772–4777. https://doi.org/10.1021/la703864a.
(57) Bloch, E. D.; Queen, W. L.; Krishna, R.; Zadrozny, J. M.; Brown, C. M.; Long, J. R. Hydrocarbon Separations in a Metal-Organic Framework with Open Iron(II) Coordination Sites. *Science* **2012**, *335* (6076), 1606–1610. https://doi.org/10.1126/science.1217544.

(58) Calleja, G.; Sanz, R.; Orcajo, G.; Briones, D.; Leo, P.; Martínez, F. Copper-Based MOF-74 Material as Effective Acid Catalyst in Friedel–Crafts Acylation of Anisole. *Catal. Today* **2014**, *227*, 130–137. https://doi.org/10.1016/j.cattod.2013.11.062.
(59) Ruano, D.; Díaz-García, M.; Alfayate, A.; Sánchez-Sánchez, M. Nanocrystalline M-MOF-74 as Heterogeneous Catalysts in the Oxidation of Cyclohexene: Correlation of the Activity and Redox Potential. *ChemCatChem* **2015**, *7* (4), 674–681. https://doi.org/10.1002/cctc.201402927.
(60) Queen, W. L.; Hudson, M. R.; Bloch, E. D.; Mason, J. A.; Gonzalez, M. I.; Lee, J. S.; Gygi, D.; Howe, J. D.; Lee, K.; Darwish, T. A.; et al. Comprehensive Study of Carbon Dioxide Adsorption in the Metal–organic Frameworks M2(dobdc) (M = Mg, Mn, Fe, Co, Ni, Cu, Zn). *Chem. Sci.* **2014**, *5* (12), 4569–4581. https://doi.org/10.1039/C4SC02064B.
(61) Garzón-Tovar, L.; Carné-Sánchez, A.; Carbonell, C.; Imaz, I.; Maspoch, D. Optimised Room Temperature, Water-Based Synthesis of CPO-27-M Metal–organic Frameworks with High Space-Time Yields. *J. Mater. Chem. A* **2015**, *3* (41), 20819–20826. https://doi.org/10.1039/C5TA04923G.
(62) Juanhuix, J.; Gil-Ortiz, F.; Cuní, G.; Colldelram, C.; Nicolás, J.; Lidón, J.; Boter, E.; Ruget, C.; Ferrer, S.; Benach, J. Developments in Optics and Performance at BL13-XALOC, the Macromolecular Crystallography Beamline at the Alba Synchrotron. *J. Synchrotron Radiat.* **2014**, *21* (4), 679–689. https://doi.org/10.1107/S160057751400825X.
(63) Kabsch, W. XDS. *Acta Crystallogr. D Biol. Crystallogr.* **2010**, *66* (2), 125–132. https://doi.org/10.1107/S0907444909047337.
(64) Sheldrick, G. M.; Dauter, Z.; Wilson, K. S.; Hope, H.; Sieker, L. C. The Application of Direct Methods and Patterson Interpretation to High-Resolution Native Protein Data. *Acta Crystallogr. D Biol. Crystallogr.* **1993**, *49* (1), 18–23. https://doi.org/10.1107/S0907444992007364.
(65) Sheldrick, G. M. SHELXT – Integrated Space-Group and Crystal-Structure Determination. *Acta Crystallogr. Sect. Found. Adv.* **2015**, *71* (1), 3–8. https://doi.org/10.1107/S2053273314026370.
(66) Farrugia, L. J. WinGX and ORTEP for Windows: An Update. *J. Appl. Crystallogr.* **2012**, *45* (4), 849–854. https://doi.org/10.1107/S0021889812029111.
(67) Spek, A. L. Structure Validation in Chemical Crystallography. *Acta Crystallogr. D Biol. Crystallogr.* **2009**, *65* (2), 148–155. https://doi.org/10.1107/S090744490804362X.

Tuning the supramolecular isomerism of MOF-74 by controlling the synthesis conditions

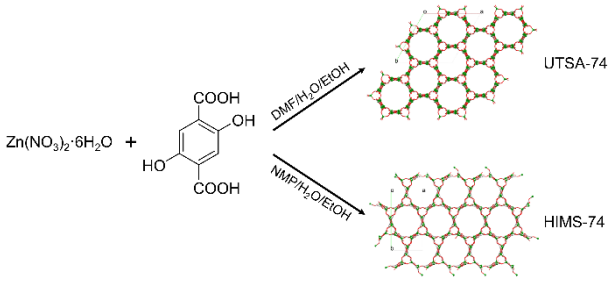

Controlled synthesis of MOFs materials with specific properties is highly relevant for practical applications and it still remains a challenging task. This work highlights the key role played by the solvents and specific modulators in the formation and stability of two isomers of the well-known MOF-74.